Bioactive Materials 19 (2023) 444–457

Contents lists available at ScienceDirect

Bioactive Materials

journal homepage: www.keaipublishing.com/en/journals/bioactive-materials

Enhanced osteoarthritis therapy by nanoengineered mesenchymal stem cells using biomimetic CuS nanoparticles loaded with plasmid DNA encoding TGF-β1

Yu Cai [a,b,1], Cuixi Wu [a,1], Qianhua Ou [a], Muhui Zeng [a,b], Song Xue [a,d], Jieli Chen [a], Yao Lu [a,b,c,*], Changhai Ding [a,e,f,**]

[a] Clinical Research Center, Zhujiang Hospital, Southern Medical University, Guangzhou, Guangdong, 510282, China
[b] Orthopedic Center, Zhujiang Hospital, Southern Medical University, Guangzhou, Guangdong, 510282, China
[c] Guangdong Key Lab of Orthopedic Technology and Implant, Guangzhou, Guangdong, 510010, China
[d] Department of Rheumatology and Immunology, Arthritis Research Institute, The First Affiliated Hospital of Anhui Medical University, Hefei, Anhui, 230032, China
[e] Guangdong Provincial Key Laboratory of Bone and Joint Degeneration Diseases, Academy of Orthopedics, Southern Medical University, Guangzhou, Guangdong, 510630, China
[f] Menzies Institute for Medical Research, University of Tasmania, Hobart, Tasmania, 7000, Australia

ARTICLE INFO

Keywords:
Osteoarthritis
Stem cell therapy
Cartilage regeneration
Cupper sulfide nanoparticles
Gene delivery

ABSTRACT

Mesenchymal stem cells (MSCs) therapy shows the potential benefits to relieve clinical symptoms of osteoarthritis (OA), but it is uncertain if it can repair articular cartilage lesions — the main pathology of OA. Here, we prepared biomimetic cupper sulfide@phosphatidylcholine (CuS@PC) nanoparticles (NPs) loaded with plasmid DNA (pDNA) encoding transforming growth factor-beta 1 (TGF-β1) to engineer MSCs for enhanced OA therapy via cartilage regeneration. We found that the NPs not only promoted cell proliferation and migration, but also presented a higher pDNA transfection efficiency relative to commercial transfection reagent lipofectamine 3000. The resultant CuS/TGF-β1@PC NP-engineered MSCs (termed CTP-MSCs) were better than pure MSCs in terms of chondrogenic gene expression, glycosaminoglycan deposition and type II collagen formation, favoring cartilage repair. Further, CTP-MSCs inhibited extracellular matrix degradation in interleukin-1β-induced chondrocytes. Consequently, intraarticular administration of CTP-MSCs significantly enhanced the repair of damaged cartilage, whereas pure MSCs exhibited very limited effects on cartilage regeneration in destabilization of the medial meniscus (DMM) surgical instability mice. Hence, this work provides a new strategy to overcome the limitation of current stem cell therapy in OA treatment through developing more effective nanoengineered MSCs.

1. Introduction

Osteoarthritis (OA), the most common chronic degenerative joint disease, is characterized by progressive destruction of articular cartilage [1,2]. Current pharmacological administration, including nonsteroidal anti-inflammatory drugs (NSAIDs), analgesics and intraarticular injection of hyaluronic acid, mainly focus on temporarily alleviating OA symptoms rather than reversing OA process [3–5]. Surgical interventions are also developed for management of cartilage defects. Microfracture (MF) technique can stimulate bone marrow mesenchymal stem cells (MSCs) to repair cartilage defects. However, MF often results in the formation of fibrocartilage but not hyaline cartilage so that cartilage degeneration only delays in the short term [6,7]. Autologous chondrocyte implantation (ACI) shows superior outcomes compared to MF in cartilage repair [8,9], while the complex procedure and unclear long-term impact on donor area limit its application [10,11]. Thus, development of new approaches that can promote cartilage regeneration is highly desired.

In recent years, stem cell therapy has drawn considerable attention in OA treatment. MSCs are multipotent progenitor cells that can be isolated

Peer review under responsibility of KeAi Communications Co., Ltd.
* Corresponding author. Clinical Research Center, Zhujiang Hospital, Southern Medical University, Guangzhou, Guangdong, 510282, China.
** Corresponding author. Clinical Research Center, Zhujiang Hospital, Southern Medical University, Guangzhou, Guangdong, 510282, China.
E-mail addresses: oayul@smu.edu.cn (Y. Lu), changhai.ding@utas.edu.au (C. Ding).
[1] Yu Cai and Cuixi Wu contributed equally to this work.

https://doi.org/10.1016/j.bioactmat.2022.04.021
Received 30 November 2021; Received in revised form 11 April 2022; Accepted 21 April 2022

from various tissues, such as bone marrow, adipose tissue and peripheral blood. These cells exhibit self-renewal and multi-lineage differentiation properties (i.e. adipocytes, osteoblasts and chondrocytes) [12]. Moreover, MSCs can selectively home to injured sites [13,14], making them promising candidates for cartilage repair. Although the underlying mechanism is not fully understood, clinical studies demonstrate that MSCs therapy is safe and may bring considerable benefits to OA patients in terms of pain relief and joint function improvement [15,16]. However, as to cartilage regeneration, several randomized controlled trials show that the effect of MSCs therapy on cartilage repair is not evident [17–21]. Given the fact that MSCs exhibit low chondrogenic differentiation efficiency in OA-related microenvironment with low chondrogenesis indicators [22], MSCs tend to differentiate into fibroelastosis-like tissue instead of hyaline cartilage [23,24]. Therefore, enhancing chondrogenic property of MSCs may boost their therapeutic effects on OA, but this remains a challenge.

Toward this goal, we synthesized cupper sulfide (CuS) nanoparticles (NPs) because our previous research showed that Cu could enhance chondrogenesis of MSCs [25]. Then CuS NPs were modified with 3-aminopropyltriethoxysilane (APTES) to obtained CuS–NH_2, facilitating the electrostatic binding with the negatively charged plasmid DNA encoding transforming growth factor-β1 (TGF-β1). Since nanoengineering of MSCs requires NPs with good biosafety and high cellular uptake rate, we further coated CuS/TGF-β1 NPs with phosphatidylcholine (PC). PC is one of the basic components of mammalian cell membrane [26], and thus biomimetic CuS/TGF-β1@PC (CTP) could effectively transfer pDNA into MSCs with low cytotoxicity. The CuS/TGF-β1@PC NP-engineered MSCs (termed CTP-MSCs) exhibited enhanced cell migration, chondrogenesis, and inhibition on extracellular matrix (ECM) degradation compared to pure MSCs. More importantly, intraarticular injection of CTP-MSCs in OA mice model showed that these MSCs could significantly promote cartilage repair, resulting in a successful OA therapy.

2. Experimental section

2.1. Synthesis of CuS/TGF-β1 NPs

CuS NPs were synthesized following our previously reported methods with modifications [27,28]. Briefly, $Cu(NO_3)_2$, L-cysteine and $Na_2S_2O_3{\cdot}5H_2O$ with the ratio of 1:3:3 were dissolved and reacted in 90 °C for 2 h. Then CuS NPs were functionalized with amino group (CuS–NH_2) by reacting with (3-aminopropyl)triethoxysilane (APTES). To obtain CuS/TGF-β1 (CT) NPs, negative charged TGF-β1 pDNA (1 μg; purchased from GenePharma, Shanghai, China) was mixed and bonded with CuS–NH_2 NPs (10, 20, and 30 μg, respectively) via electrostatic binding [29].

2.2. Synthesis of CuS/TGF-β1@PC NPs

For phosphatidylcholine (PC) modification, 1 mg of PC was dissolved in absolute ethanol. The PC solution was evaporated to remove ethanol and formed a thin film. Then the as-prepared CuS/TGF-β1 NPs solution were mixed with PC film at a mass ratio of 3:1. The mixture were shaken gently for re-dispersion and subjected to sonication for 15 min. After centrifugation and washing with distilled water, the final CuS/TGF-β1@PC NPs were obtained.

2.3. Characterization of the NPs

Morphology of CuS and CuS@PC NPs were observed by high-resolution transmission electron microscopy. The crystalline structure of the CuS NPs was detected by X-ray diffraction (XRD). Zeta potential of the NPs before and after binding with pDNA was measured. Fourier transform infrared spectroscopy (FTIR) spectra of the different samples were obtained using an FTIR spectrometer. Gel electrophoresis analysis was conducted to study pDNA binding efficiency, and the reaction supernatants of CuS/TGF-β1 NPs were added into 1% agarose gel with ethidium bromide (0.1 μg/mL). The samples were run at 120 V for 40 min to detect the unbinding free pDNA in the supernatants.

2.4. Cytotoxicity and preparation of the NP-engineered MSCs

MSCs derived from bone marrow of C57 mice were cocultured with CuS and CuS@PC NPs with gradient concentrations (0, 12.5, 25, 50, 100, and 150 μg/mL), respectively. After 24 h, standard cell counting kit-8 (CCK-8) assay (APExBio, USA) were performed to test cytotoxicity of the NPs. The cell viability was calculated as followed: cell viability (%) = $(OD_{sample} - OD_{cck})/(OD_{control} - OD_{cck}) \times 100\%$, where OD_{sample} was the OD value of NP-cocultured MSC group, $OD_{control}$ was the OD value of pure MSC group, and OD_{cck} was the OD value of the culture medium containing CCK-8 solution.

To prepare the NP-engineered MSCs, we first studied the optimal concentration and incubation time of the NPs for nano engineering. MSCs were cocultured with Cy5.5-labeled CuS and CuS@PC NPs with gradient concentrations (0, 12.5, 25, 50, 100, and 150 μg/mL) for 2 h. After washing with PBS for three times, Cy5.5 positive MSCs were detected by flow cytometry. Time-dependent cellular uptake of the NPs (25 μg/mL) was investigated. The Cu content of the NP-engineered MSCs at each time point (2, 3, and 4 h) was detected by inductively coupled plasma-mass spectrometry (ICP-MS).

Then we incubated MSCs with CuS, CuS@PC, CuS/TGF-β1, CuS/TGF-β1@PC NPs (25 μg/mL, 2 h) to obtain C-MSCs, CP-MSCs, CT-MSCs, and CTP-MSCs, respectively. The free NPs were removed by repeatedly washing of PBS.

In addition, flow cytometry was conducted to identify the typical surface marker of MSCs after nanoengineering according to the standard criteria defined by International Society for Cell Therapy (ISCT) [30].

2.5. Transwell study

Approximately 5×10^4 of the above-prepared NP-MSCs were seeded on the upper chamber of a transwell system and cultured with serum-free low-glucose DMEM medium. The lower chambers were filled with DMEM medium contained 10% FBS. After cultured for 24 and 48 h, MSCs in upper layer of the membrane was scraped. MSCs migrated to the lower layer were fixed with 4% paraformaldehyde and stained by 1% crystal violet. MSCs in five random microscope images were counted using Image J software.

2.6. Scratch test

Different NP-engineered MSCs were added into a 24-well plate and cultured until they completely covered the well. A scratch was made and then the MSCs were cultured for additional 24 and 48 h, respectively. The initial wound area (0 h; between white dotted lines) in each image was measured using Image J software. The wound areas at 24 h and 48 h were calculated by the same method. Then the wound healing rate was calculated using the following formulation: wound healing rate (%) = $(A_{initial} - A_{time})/A_{initial} \times 100$, where $A_{initial}$ is the initial wound area (0 h), and A_{time} is the wound area at different time points. In order to better observe cell migration, MSCs were stained with calcein-AM and observed by a fluorescence microscope. Number of the migrated cells was calculated by Image J software.

2.7. Transfection efficiency of TGF-β1 pDNA in the NP-engineered MSCs

To study the transfection efficiency of the NPs, MSCs were cocultured with different NPs (25 μg/mL) for 2 h. Commercial transfection agent liposome 3000 (lipo3000; ThermoFisher, USA) was used as a positive control group following the same transfection protocol.

Briefly, TGF-β1 pDNA was incubated with lipo3000 transfection reagent according to the manufacturer's instructions. The pDNA-loaded

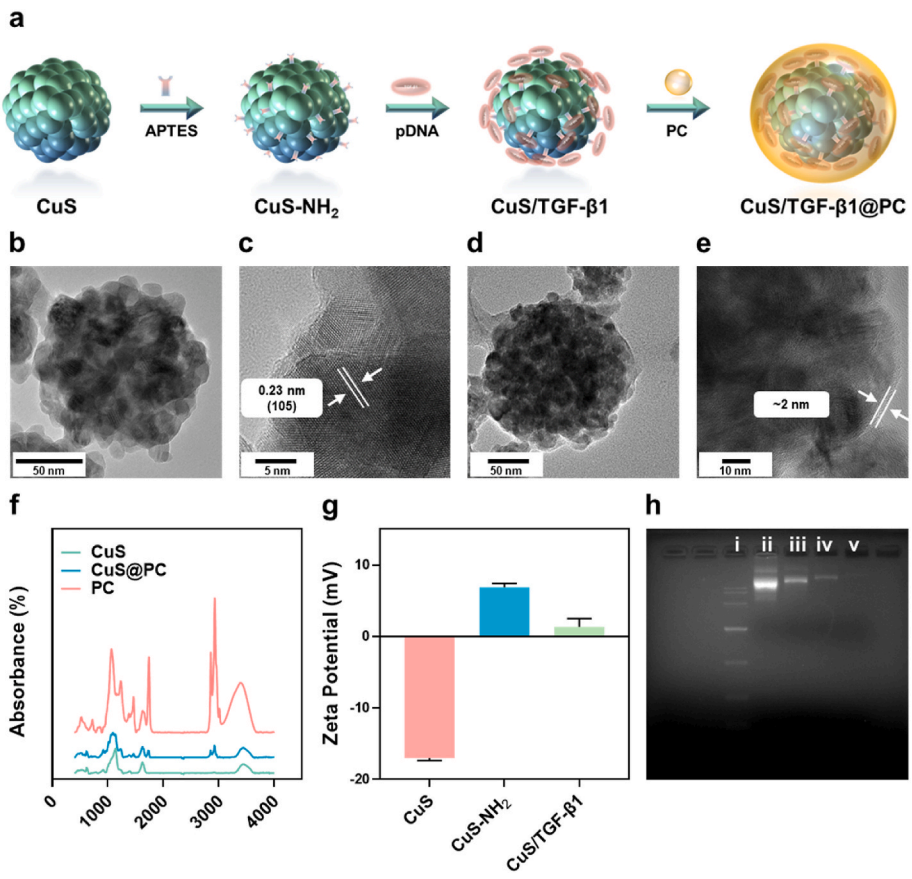

Fig. 1. Preparation and characterizations of the NPs. (a) Schematic illustration of the preparation of the NPs. CuS NPs were reacted with ATPES to obtained CuS–NH_2 NPs, and then electrostatically bonded with negatively charged TGF-β1 pDNA. Then PC was coated on the NPs for biomimetic modification. TEM images of CuS (b, c) and CuS@PC (d, e) NPs, respectively. A thin layer (~2 nm) of PC was observed on the NPs, indicating the successful surface modification of PC. (f) FTIR spectra of the NPs and PC. (g) Zeta potential of CuS, CuS–NH_2, and CuS/TGF-β1 NPs, respectively (n = 3). (h) Agarose gel electrophoresis assay of the unbinding pDNA in the supernatant after the reaction of CuS–NH_2 NPs and TGF-β1 pDNA. (i) marker; (ii) TGF-β1 pDNA; (iii-v) unbinding pDNA in the reaction of CuS–NH_2 and pDNA at the ratio of 10:1, 20:1, 30:1, respectively. Data are presented as means ± SD.

lipo3000 (containing the same amount of pDNA as 25 μg/mL of CT or CTP NPs) was cocultured with MSCs for 2 h. Then the free lipo3000 or NPs were removed by washing with PBS and MSCs were cultured for an additional 2 days.

Then gene expression of TGF-β1 in these MSCs were tested after 2 days of culture by quantitative reverse transcription polymerase chain reaction (RT-qPCR) and a $2^{-\Delta\Delta CT}$ method was used to determine the relative mRNA expression level as we previously reported [31]. Protein expression of TGF-β1 was also study by Western blot (WB). After 3 days of incubation, cells were collected and lysed (RIPA Lysis Buffer, P0013B, Beyotime, China). Protein was extracted (RIPA Lysis Buffer, P0013B, Beyotime, China) and quantified (BCA protein assay kit, P0010, Beyotime, China) for further evaluation. Samples with equal concentration were separated by SDS-PAGE. The proteins were transferred to polyvinylidene difluoride membranes, blocked, and incubated with TGF-β1 primary antibody (ab215715, Abcam, UK) overnight. The dilution ratio of primary antibodies is 1:1000. After conjugated with peroxidase secondary antibody (1:2000; SA00001-2, Proteintech, USA), TGF-β1 protein was detected using an enhanced chemiluminescence kit (Millipore, USA). We further determined TGF-β1 content in the culture supernatants by an enzyme linked immunosorbent assay (ELISA) kit (MEIMIAN, China) according to the manufacturer's instructions.

2.8. Chondro-inductivity of the NP-engineered MSCs

The NP-engineered MSCs were chondrogenically cultured with chondrogenic media (Cyagen Biosciences) for 7 days. The expression levels of chondrogenic genes including SRY-box transcription factor 6 (SOX-6), SOX-9, aggrecan and type II collagen (Col-2a1) were analyzed by RT-qPCR. The gene expression levels of Col-1a1 and Col-1a2 (fibrotic markers) as well as Col-10a1 and MMP-13 (hypertrophic markers) were detected.

Moreover, different MSCs were seeded in a 12-well plate and chondrogenically induced as described above for 7 and 14 days. Then glycosaminoglycan (GAG) formation was detected using alcian blue staining. We further induced the NP-engineered MSCs into cell pellets according to the manufacturer's instructions.

Briefly, MSCs (4×10^5 cells) were suspended in a 15 mL centrifugal tube. After centrifugation at 250 *g* for 4 min, the supernatant was removed and MSCs chondrogenic medium (MUXMX-90041, Cyagen Biosciences) was slowly added into the tube without resuspending the cells. After incubated for an additional 2 days, cell pellets were formed in the bottom of the tube. The chondrogenic medium was changed every three days. After 4 weeks of incubation, cell pellets were fixed, embedded in paraffin, and cut into sections. Type II collagen (Col-2) expression was detected by immunohistochemistry.

2.9. Effects of the NP-engineered MSCs on OA chondrocytes

To study the interaction between the NP-engineered MSCs and OA chondrocytes, we incubated ATDC5 mouse chondroblasts cell line with IL-1β (10 ng/mL) for 24 h to simulate OA chondrocytes in vitro. We seeded the NP-engineered MSCs on the upper chamber of a transwell system while the IL-1β induced ATDC5 cells were seeded on the lower chamber. After incubation of 24 h, ATDC5 cells were collected and their RNA was isolated. Then mRNA expression levels of non-specific matricial gene Col-1a1, specific matricial gene Col-2a1, matrix metalloproteinase-3 (MMP-3), MMP-13 and tumor necrosis factor-α (TNF-α) were determined by RT-qPCR. Moreover, supernatants in the lower chamber were also collected after incubation of 48 h. Contents of MMP-13 and TNF-α in supernatants were tested by ELISA sets (MEIMIAN, China) according to the manufacturer's instructions.

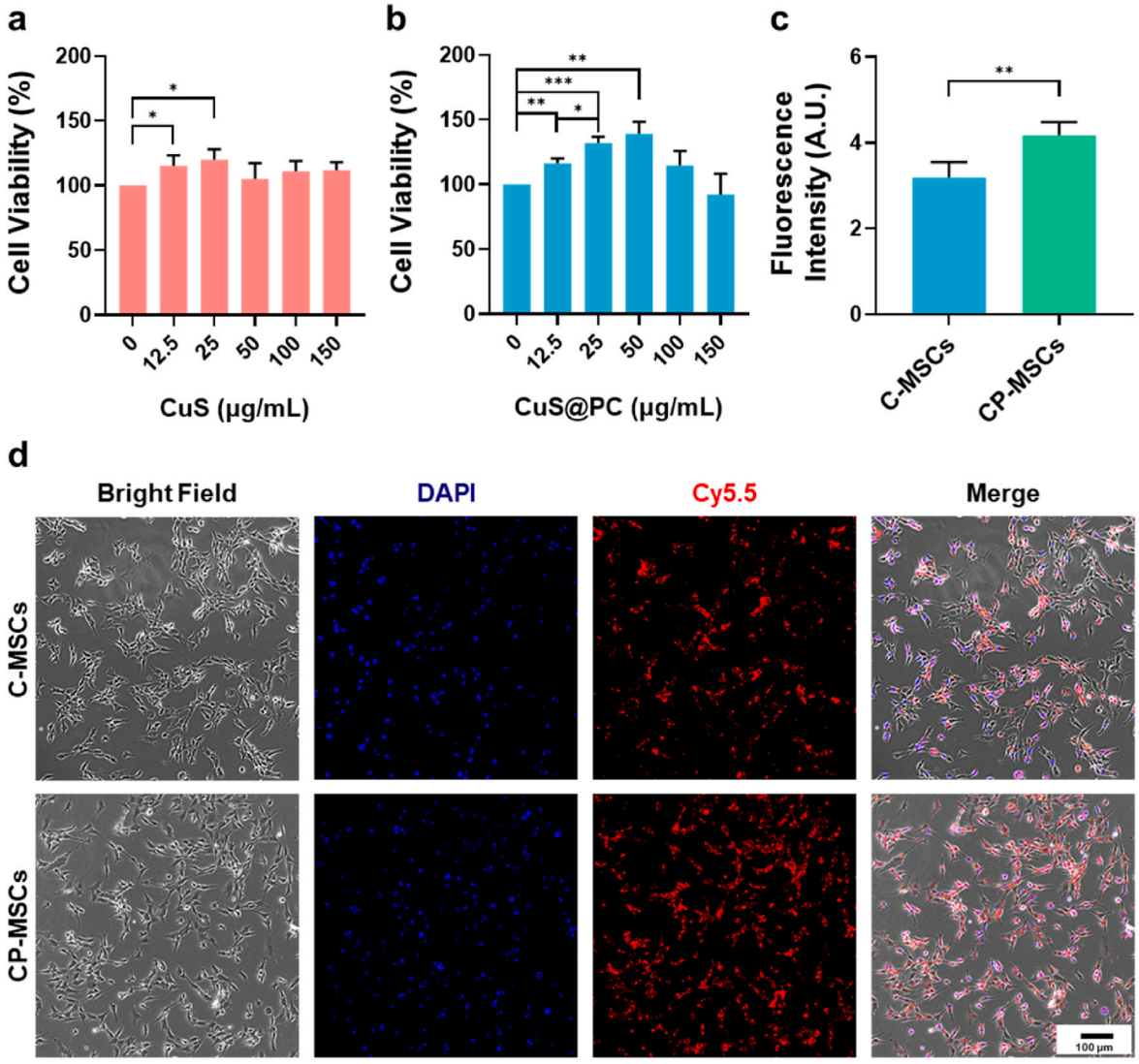

Fig. 2. Cytotoxicity and cellular uptake of the NPs. Cell viability of MSCs after cocultured with (a) CuS and (b) CuS@PC NPs with various concentration for 24 h. (c) Fluorescence intensity of MSCs engineered with the Cy5.5-labeled NPs. Fluorescence intensity was measured from five images acquired from random positions of the samples. (d) Representative fluorescent images of MSCs engineered with the Cy5.5-labeled NPs. Cellular uptake of the NPs was higher (stronger red fluorescence) in CP-MSCs relative to C-MSCs. Data are presented as means ± SD. *$p < 0.05$, **$p < 0.01$, ***$p < 0.001$, and ****$p < 0.0001$.

2.10. Establishment of early OA model

All animal experimental procedures were approved by Institutional Animal Care and Use Committee (IACUC) of Zhujiang Hospital, Southern Medical University (LAEC-2020-077). Male C57BL/6 mice at age of 8 weeks were induced into OA model by surgical destabilization of the medial meniscus (DMM) as we previously reported [32]. Briefly, after anesthetization, a medial capsular incision was made on the right knee joint of mice. Then the medial meniscus supporting ligament was resected and the medial meniscus was displaced medially. After 2 weeks post-surgery, DMM mice were randomly divided into five treatment groups ($n = 12$) as followed: 1) PBS, 2) MSCs, 3) CP-MSCs, 4) CT-MSCs, and 5) CTP-MSCs. A total of 10 μL of different solutions (PBS or suspension of different MSCs with a cell number of 1×10^5) were slowly injected into right knees of DMM mice biweekly. A sham group was set as the normal control by only exposing knee joint but not cutting the ligament. Mice were sacrificed at 6 and 10 weeks after initial surgery, respectively. The right knee joints of mice were harvested for further evaluation.

To investigate the in vivo distribution of the MSCs, CTP-MSCs and pure MSCs were stained with DiD cell-labeling solution (AAT Bioquest, USA). The DiD-labeled MSCs (with a cell number of 1×10^5) were intraarticularly injected into right knees of the mice models. After 48 h, the joint samples were collected, fixed and decalcified. The sections were stained by DAPI (for nuclei staining) and observed by a fluorescence microscope.

2.11. Histological study and immunofluorescence staining

The joint samples were fixed and decalcified. The sections were stained with Safranin-O/fast green and toluidine blue, respectively. Semi-quantitative analysis of the sections was performed according to Osteoarthritis Research Society International (OARSI) scores [33].

In addition, we performed immunofluorescence staining to detect protein expression of Col-2, TGF-β1 and MMP-13. The sections were incubated with rabbit anti-mouse primary antibodies (1:500; ab34712, ab39012, Abcam, UK and 21898-1-AP, Proteintech, USA, respectively) at 4 °C overnight, and then stained with Alexa Fluor® 647-conjugated donkey anti-rabbit secondary antibody (1:1000; ab150075, Abcam, UK) and DAPI.

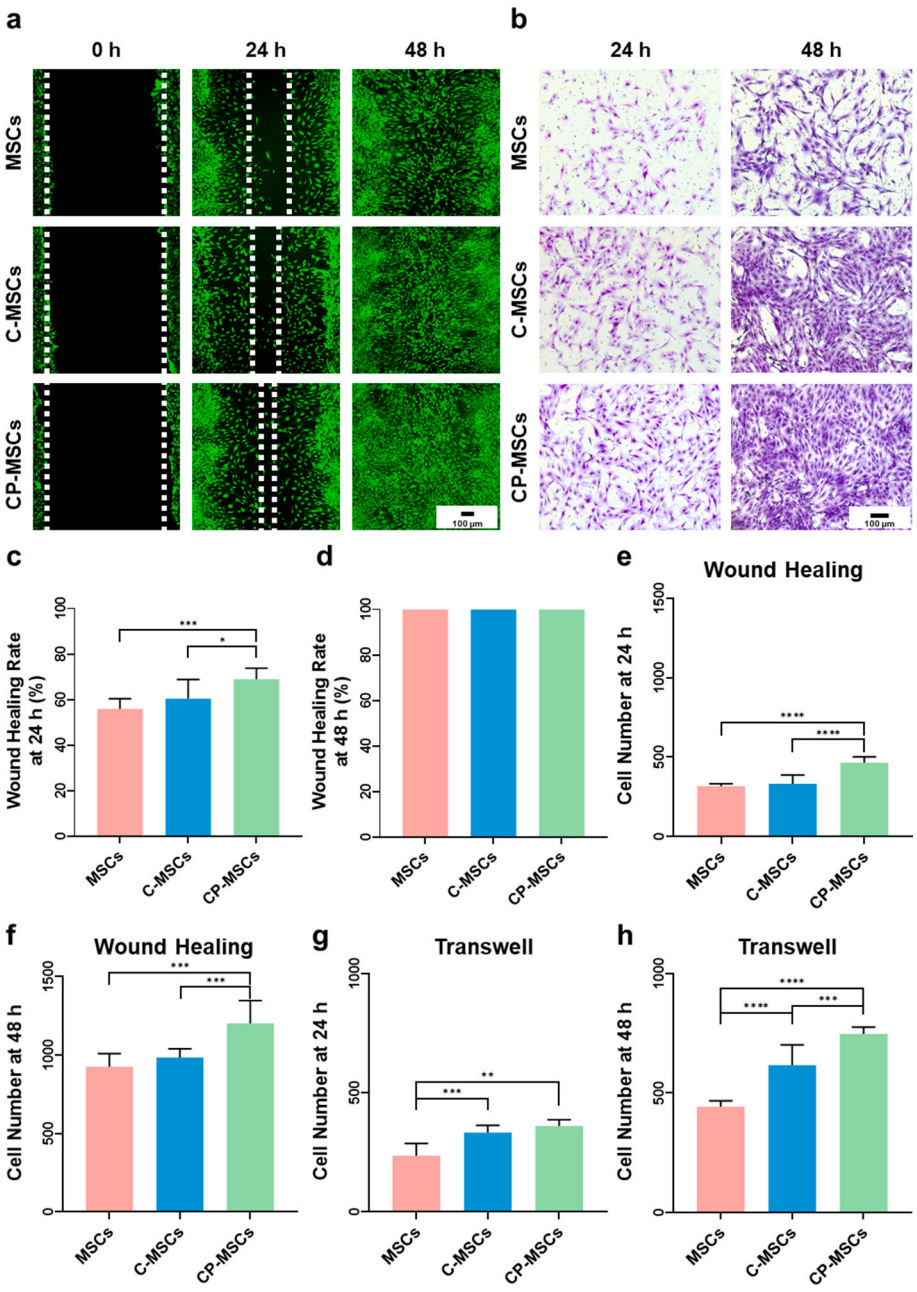

Fig. 3. In vitro migration ability of the NP-engineered MSCs. (a) Representative fluorescent images of wound healing. MSCs were visualized by calcein-AM staining. (b) Representative images of migrated MSCs. MSCs were stained by crystal violet. (c, d) Wound healing rate in different MSCs after 24 h and 48 h, respectively. (e, f) Number of MSCs in the scratch areas at 24 h and 48 h, respectively (n = 5; wound healing study). (g, h) Number of the migrated MSCs calculated from random positions of the samples (n = 5; transwell study). Data are presented as means ± SD. *p < 0.05, **p < 0.01, ***p < 0.001, and ****p < 0.0001.

2.12. Biosafety of the NP-engineered MSCs

Main organs including heart, spleen, lung, liver, and kidney of mice were collected after treatments and subjected to hematoxylin-eosin (H&E) staining. Serum of mice were also collected and blood biochemistry test was conducted.

2.13. Statistical analysis

Data are presented as mean ± standard deviation (SD). Statistical comparisons among multiple treatment groups were measured using one-way analysis of variance (ANOVA) followed by post hoc multiple comparison (LSD test). A p-value less than 0.05, 0.01, 0.001, and 0.0001 was regarded statistically significant with an increasing level of the significance.

3. Results

3.1. Preparation and characterization of CTP NPs

We prepared CuS NPs according to our previously reported methods [28]. TEM image (Fig. 1b) showed that CuS NPs had a sphere shape with a size of ~100 nm. XRD results (Fig. S1) confirmed that the as-prepared CuS NPs were standard CuS (PDF#06–0464). The interplanar crystal spacing was 0.23 nm, corresponding well with the d-spacing for (105) plane of CuS nanocrystals and XRD results (Fig. 1c). Then CuS NPs were reacted with APTES to get CuS–NH_2 NPs, favoring further binding with the negative charged pDNA (Fig. 1a). Zeta potential of the NPs increased from −17 mV to 6.8 mV after amino modification, and then decreased after binding with negative pDNA (Fig. 1g). To study the optimal reaction ratio of CuS–NH_2 NPs and pDNA, we mixed the NPs with pDNA at a various mass ratio of 30:1, 20:1, 10:1, respectively. We found that free pDNA gradually decreased along with the increasing of

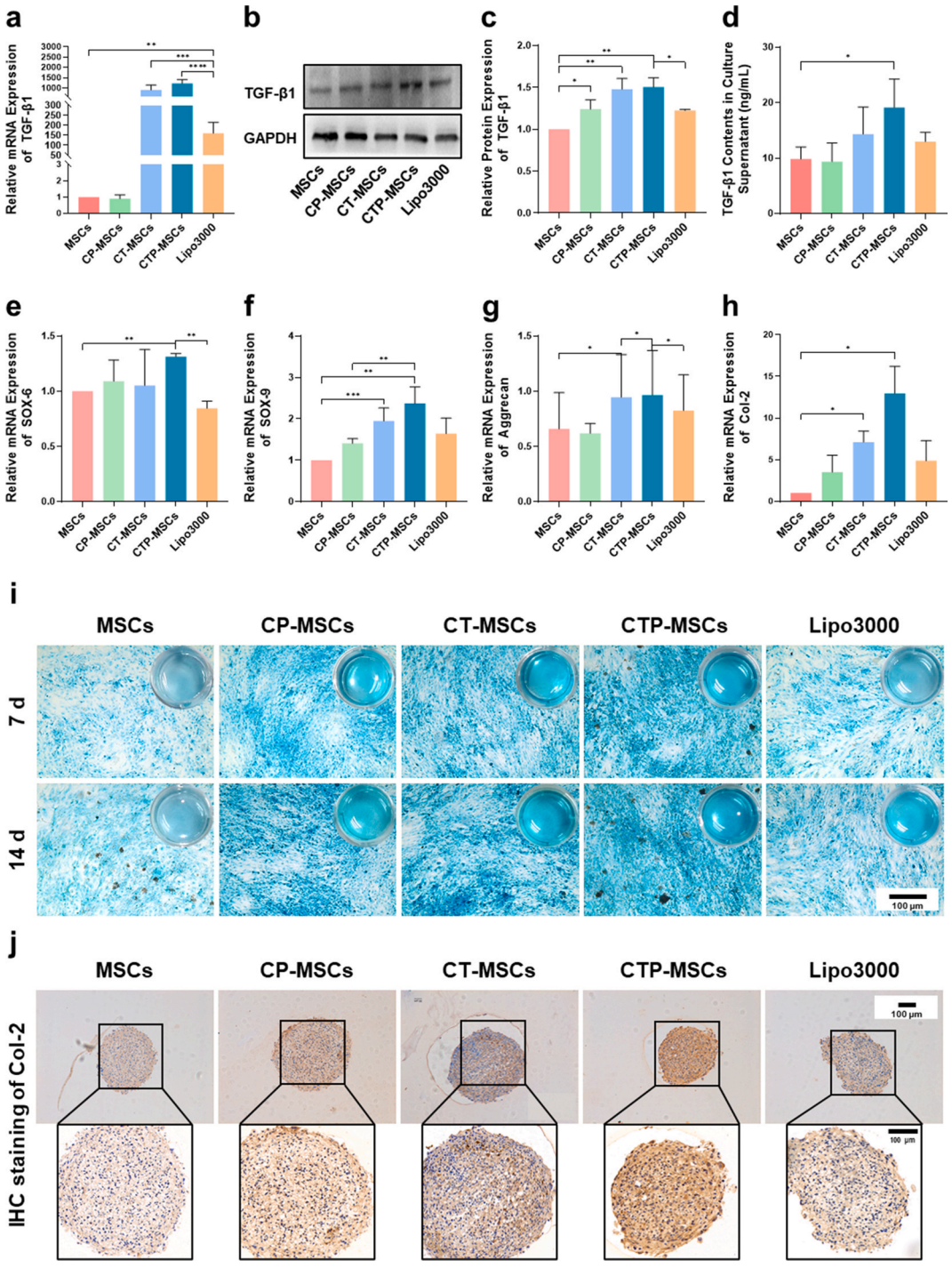

Fig. 4. Transfection of TGF-β1 pDNA and chondrogenesis of the NP-engineered MSCs. (a) Relative mRNA expression of TGF-β1 in different MSCs after 2 days of culture (n = 3). Commercial transfection agent lipo3000 was set as a positive control. Protein expression (b) and quantify analysis (c) of TGF-β1 in the MSCs after 3 days of culture (n = 3). (d) TGF-β1 contents in culture supernatant (n = 3). (e–h) Relative mRNA expression of SOX-6, SOX-9, aggrecan, and Col-2a1 in the MSCs, respectively (n = 3). (i) Glycosaminoglycan (GAG) deposition in the MSCs (visualized by alcian blue staining). Inserted images: overall photographs of the culture wells. (j) Immunohistochemistry (IHC) staining of Col-2 protein in cell pellets induced by different MSCs. Data are presented as means ± SD. *$p < 0.05$, **$p < 0.01$, ***$p < 0.001$, and ****$p < 0.0001$.

NP-concentration (Fig. 1h). Moreover, free pDNA was disappeared when the ratios were 30:1, demonstrating that pDNA was completely bonded on the NPs. We chose to use the ratio of 20:1 in our further study. Finally, CuS/TGF-β1 were coated with PC to get the CuS/TGF-β1@PC NPs (termed CTP). A thin layer could be clearly observed on the NPs after PC coating and its thickness was approximately 2 nm (Fig. 1d and e). FTIR analysis showed that CuS@PC NPs exhibited both characteristic peaks of CuS and PC, indicating the successful coating of PC on the CuS NPs (Fig. 1f).

3.2. Preparation and characterization of CTP-MSCs

We first performed a standard CCK-8 assay to examine the cytotoxicity of the NPs toward MSCs. Both CuS and CuS@PC group were

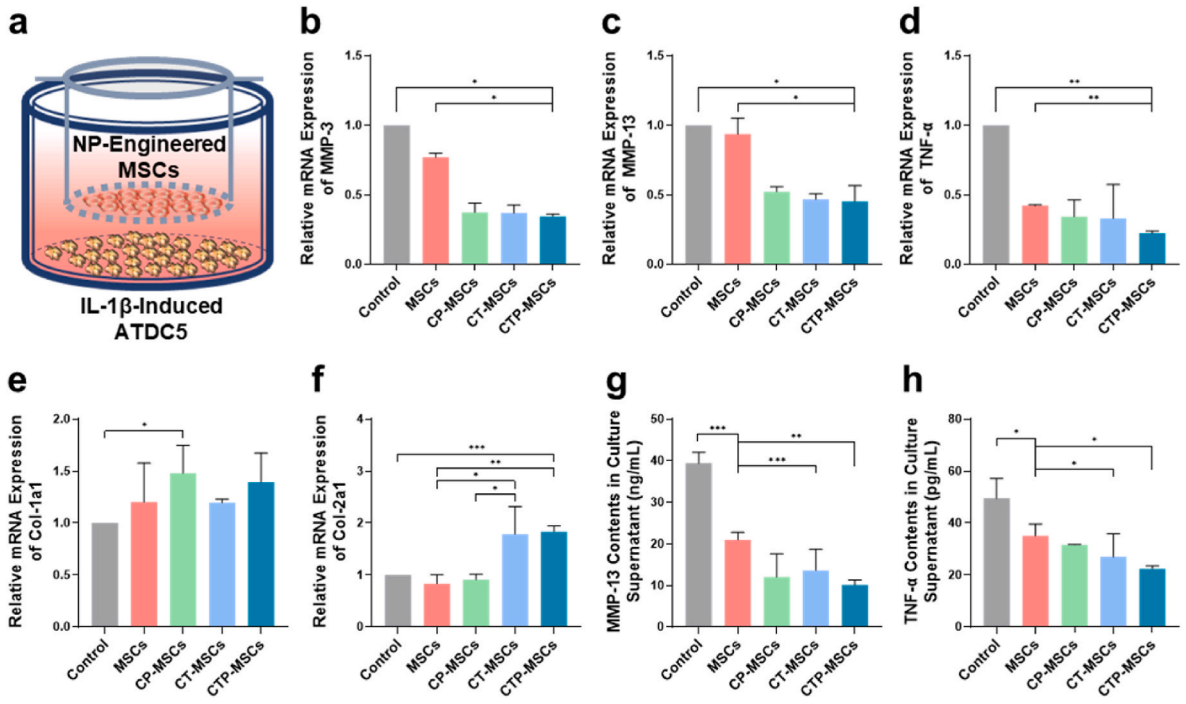

Fig. 5. Interaction of the NP-engineered MSCs with OA chondrocytes. (a) Schematic illustration of the transwell assay. Relative mRNA expression of (b) MMP-13, (c) MMP-3, (d) TNF-α, (e) Col-1a1 and (f) Col-2a1 in IL-1β-induced ATDC5 cells (to stimulate OA chondrocytes) after cocultured with different MSCs for 24 h. (g, h) MMP-13 and TNF-α contents in culture supernatants of the lower chamber, respectively. The NP-engineered MSCs were seeded on the upper chamber while the IL-1β-induced ATDC5 cells were seeded on the lower chamber. IL-1β-induced ATDC5 without any treatment was set as control group. Data are presented as means ± SD (n = 3). *p < 0.05, **p < 0.01, ***p < 0.001.

biocompatible within 150 μg/mL (Fig. 2a and b). Interestingly, cell proliferation significantly enhanced when MSCs were cocultured with 25 μg/mL of both NPs. Next, we studied the nanoengineering procedure in detail to determine the optimal NP-concentration and transfection time. We found that the cellular uptake rate of the NPs was similar in MSCs cocultured with 25, 50, 100 and 150 μg/mL of Cy5.5-labeled NPs (Fig. S2, determined by flow cytometry). The cellular uptake of CuS@PC NPs was higher relative to CuS NPs when the NP concentrations were 12.5 and 25 μg/mL (Fig. S2). Moreover, contents of the CuS NPs (~2.8 μg per 10^5 cells, determined by ICP-MS) showed no significant differences along with different incubation time points (Fig. S3a). The contents of Cu were higher in CuS@PC NP group relative to CuS NP group (Fig. S3b). Therefore, 25 μg/mL and 2 h was defined as the best NP-concentration and incubation time, respectively, for MSC nanoengineering. Additionally, we analyzed the presence or absence of CD44, CD73, CD90, CD105 and CD45 of the nanoengineered-MSCs [30]. The flow cytometry results demonstrated that engineering of the NPs did not influence normal phenotypes of MSCs (Fig. S4).

We further compared the cellular uptake of the CuS and CuS@PC NPs (labeled by Cy5.5). As shown in Fig. 2d, stronger red fluorescence intensity was observed in CuS@PC group compared to CuS group, which was also confirmed by fluorescence intensity analysis (Fig. 2c). As a crucial component of the cell membrane, PC is considered to be a safe excipient for drug delivery. Moreover, lecithin NPs (which contain PC) could promote drug bioavailability without influencing the fluidity of cell membrane [34,35]. Therefore, PC modification could promote engineering of the NPs into MSCs for efficient delivery of pDNA.

We performed a scratch test to detect the migration of the NP-engineered MSCs. Scratches in the NP-engineered MSCs (visualized by calcein-AM) healed faster than that of pure MSC group after 24 h (Fig. 3a). Specifically, CP-MSCs exhibited the best migratory ability and had the highest cell number among all groups (Fig. 3c and e). After 48 h, although all scratches were completely healed in different groups (Fig. 3d), cell number was significantly higher in CP-MSCs group (Fig. 3f).

We used a transwell system to further investigate the migration of the NP-engineered MSCs and similar results were found. After 24 h and 48 h of incubation, much more NP-engineered MSCs (visualized by crystal violet staining, Fig. 3b) migrated from the upper layer to the lower layer of the chamber (Fig. 3g and h), indicating that MSCs obtained stronger migration and proliferation properties after nanoengineering. These results were in accordance with our previous reports that Cu could promote cell proliferation and wound healing [36].

3.3. pDNA delivery efficiency and chondrogenesis of CTP-MSCs

To study the pDNA delivery efficiency in the NP-engineered MSCs, we performed RT-qPCR to detect TGF-β1 expression (Fig. 4a). Commercial lipo3000 was set as a positive control. Pure MSCs and CP-MSCs were set as control groups. We found that the mRNA expression level of TGF-β1 were significantly up-regulated in CT-MSCs, CTP-MSCs, and lipo3000 groups. Impressively, TGF-β1 levels were approximately 7-folds higher in CT-MSCs and CTP-MSCs than the commercial lipo3000 group. WB (Fig. 4b and c) and ELISA (Fig. 4d) also indicated that TGF-β1 expression level was highest in CTP-MSCs among all groups. These above-mentioned results demonstrated that MSCs was successfully transfected by pDNA and expressed bioactive TGF-β1 though our nanoengineering strategy.

Encouraged by the high TGF-β1 expression ability of the NP-engineered MSCs, we explored their chondrogenic differentiation. After 7 days of chondrogenic induction, mRNA expression levels of all chondrogenic markers including SOX-6, SOX-9, aggrecan, and Col-2a1 were significantly increased in CTP-MSCs compared to pure MSCs (Fig. 4e–h). CP-MSCs, CT-MSCs and lipo3000 also enhanced chondrogenesis to some extent because Cu could promote cartilage differentiation and TGF-β1 pDNA had been transfected into MSCs. The expression of fibrotic genes (Col-1a1 and Col-1a2) and hypertrophic genes (Col-10a1 and MMP-13) were higher in CP-MSCs relative to pure MSCs. In

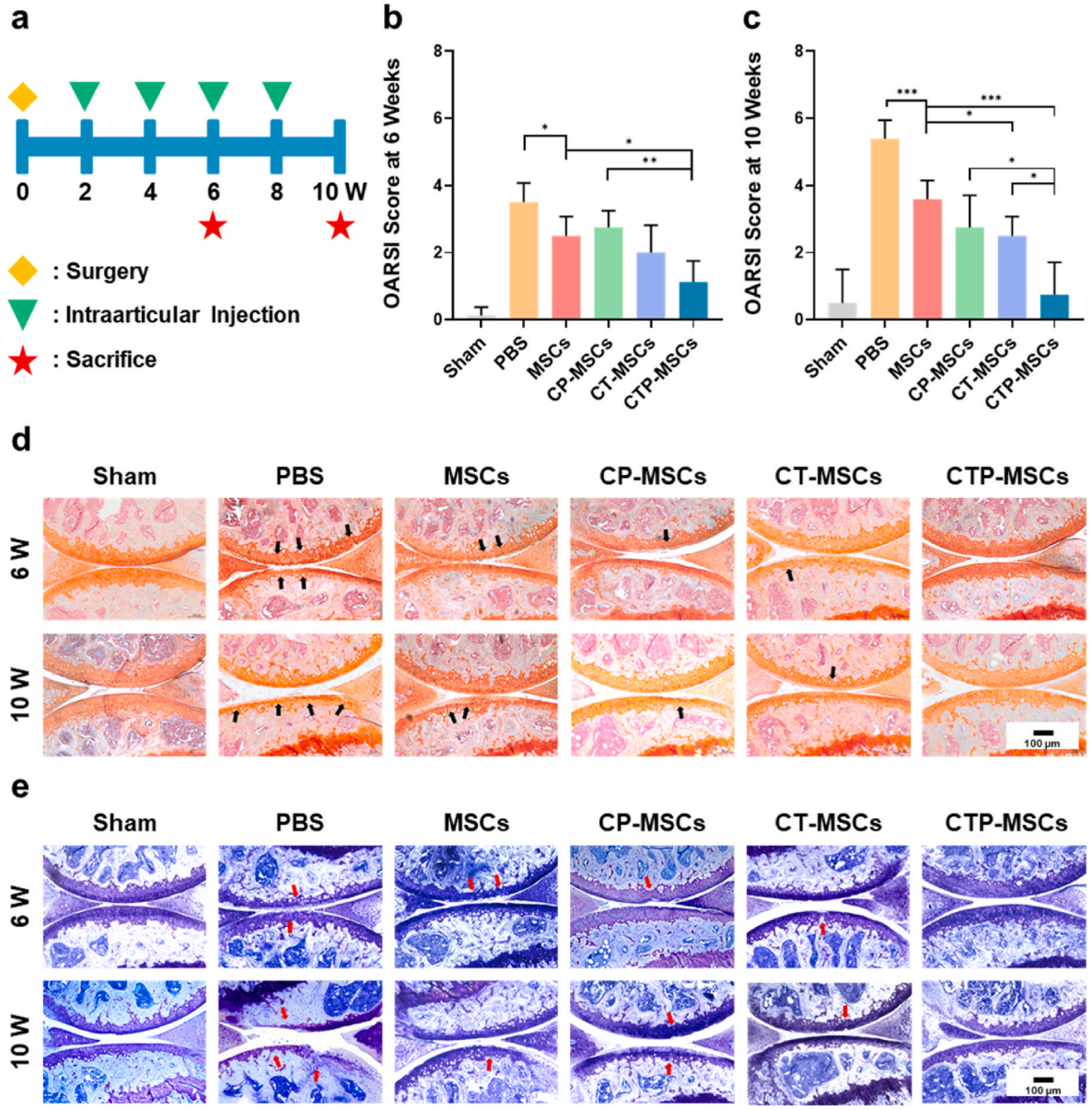

Fig. 6. Therapeutic effects of the NP-engineered MSCs on DMM mice. (a) Schematic diagram of the experimental design. After two weeks post-surgery, different MSCs or PBS were intraarticularly injected into the knee joints of mice every two weeks. The knee joints were collected at 6 weeks and 10 weeks post-surgery, respectively (n = 6 mice per group at each time point). (b, c) OARSI scores were measured according to the histological analysis of the samples collected at 6 weeks and 10 weeks post-surgery, respectively. Representative images of (d) Safranin-O/Fast green staining and (e) Toluidine blue staining of the knee joints after different treatments. Cartilage lesions were highlighted by black arrows in (d) and red arrows in (e), respectively. Data are presented as means ± SD. *p < 0.05, **p < 0.01, ***p < 0.001.

contrast, the fibrotic and hypertrophic genes expression had no difference between CTP-MSCs and pure MSCs (Fig. S5).

Then we analyzed GAG deposition in different MSCs by alcian blue staining (Fig. 4i). More cells were dyed into blue color in the NP-engineered MSCs groups compared to pure MSCs. Moreover, the blue color was deeper in CTP-MSCs than those of CP-MSCs, CT-MSCs, and lipo3000 groups. GAG is an important component of the chondrocytes and one of the most characteristic expression products in cartilage [37]. The staining degree reflected that more GAG was synthesized in CTP-MSCs.

Further, we induced the NP-engineered MSCs into cell pellets for 4 weeks and detected Col-2 formation by IHC staining (Fig. 4j). Cell pellets of the NP-engineered MSCs were stained into deeper brown color (Col-2 expression) than those of MSCs and lipo3000 groups. Moreover, the brown color was deepest in cell pellet of CTP-MSCs among all groups. Hence, CTP-MSCs exhibited an enhanced chondrogenic differentiation property compared to pure MSCs.

3.4. Interaction of the NP-engineered MSCs with OA chondrocytes

We incubated ATDC5 chondroblasts with IL-1β for 24 h to simulated OA chondrocytes in vitro [32]. To determine whether NP-engineered MSCs could alleviate the matrix degradation of OA, MSCs were seeded on the upper chamber and the IL-1β-induced ATDC5 cells were seeded on the lower chamber using a transwell system (Fig. 5a). RT-qPCR results revealed that the mRNA expression level of MMP-3, MMP-13, and TNF-α in OA chondrocytes were significantly inhibited by the NP-engineered MSCs (Fig. 5b–d). In addition, the expression level of non-specific matricial gene Col-1a1 of OA chondrocytes was not significantly different between the NP-engineered MSCs and pure MSCs

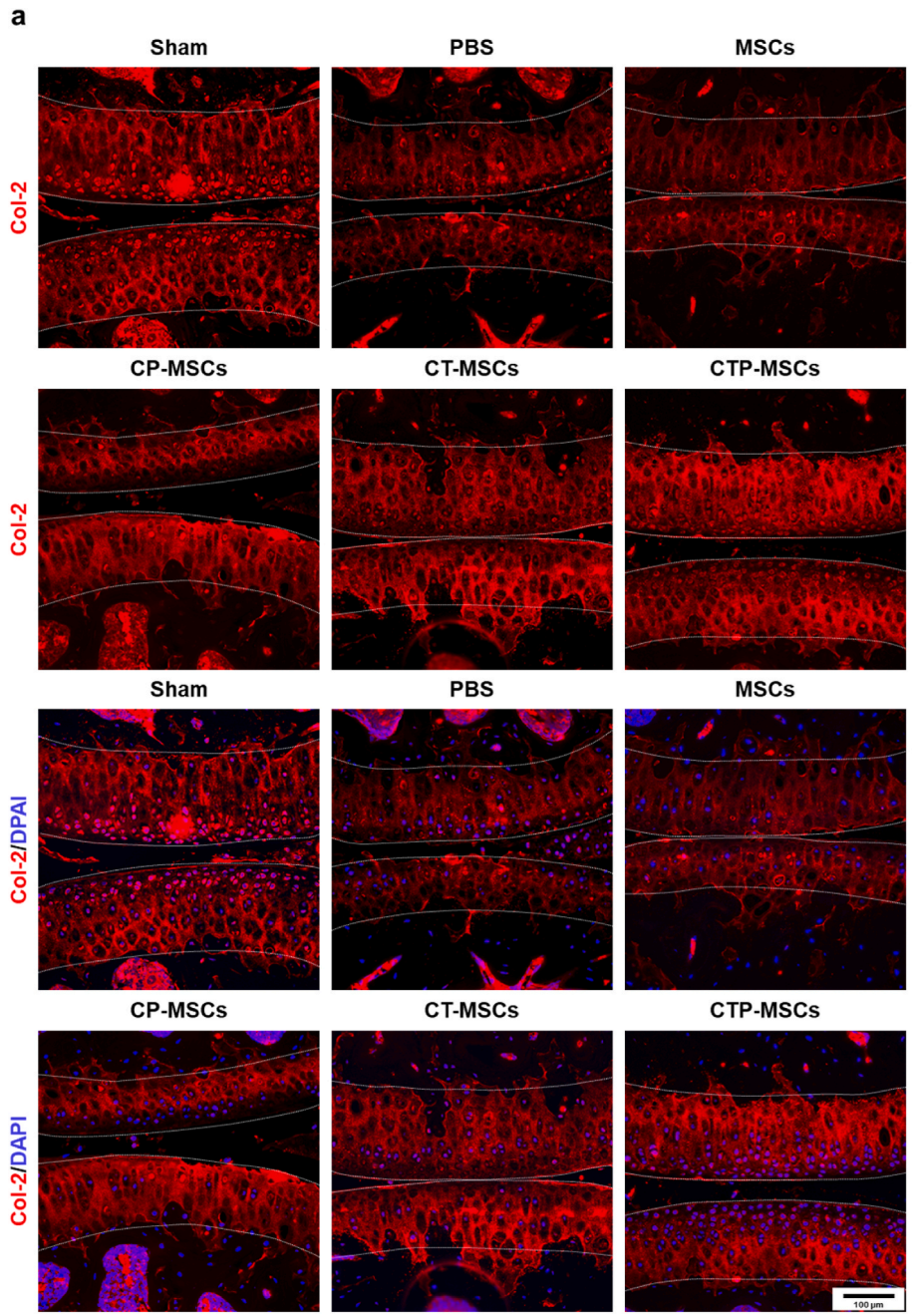

Fig. 7. Immunofluorescence staining of Col-2 in knee joints at 10 weeks post-surgery. The expression of Col-2 was higher in NP-engineered MSCs groups relative to MSCs and PBS groups. The cartilage areas were highlighted by white dotted lines.

groups (Fig. 5e). Remarkably, specific matricial gene Col-2a1 expression was significantly increased in OA chondrocytes treated with CT-MSCs and CTP-MSCs (Fig. 5f).

Moreover, we collected the culture media in the lower chamber and found that the contents of matrix degradation marker MMP-13 and inflammatory marker TNF-α in all MSCs groups were decreased (Fig. 5g and h).

3.5. *Therapeutic effect and safety of the NP-engineered MSCs on mice with early OA*

We established early OA model (2 weeks after DMM surgery) and intraarticularly injected different MSCs biweekly into the knees of OA mice (Fig. 6a). At 6 weeks post-surgery, safranin-O/fast green staining (Fig. 6d) and Toluidine blue staining (Fig. 6e) showed that articular cartilage was eroded in PBS group. Mild cartilage damage (highlighted by arrows) was observed in MSCs, CP-MSCs, and CT-MSCs groups. By contrast, cartilage of mice treated with CTP-MSCs was effectively protected and had no obvious difference with mice in the sham group. With the time prolongation, cartilage destruction was worsened in all groups except CTP-MSCs and sham groups at 10 weeks post-surgery. We evaluate the disease severity by OARSI score (Fig. 6b and c). The scores were similar in CTP-MSCs and sham groups. However, the scores were increased in other treatment groups over time, revealing the progression of OA.

Changes of cartilage markers Col-2 and TGF-β1 in cartilage matrix after different treatments at 10 weeks were also studied by in immunofluorescence (Figs. 7 and 8). The fluorescence intensity of these two markers were increased in all NP-engineered MSCs groups compared to MSCs and PBS groups. Meanwhile, the NP-engineered MSCs decreased

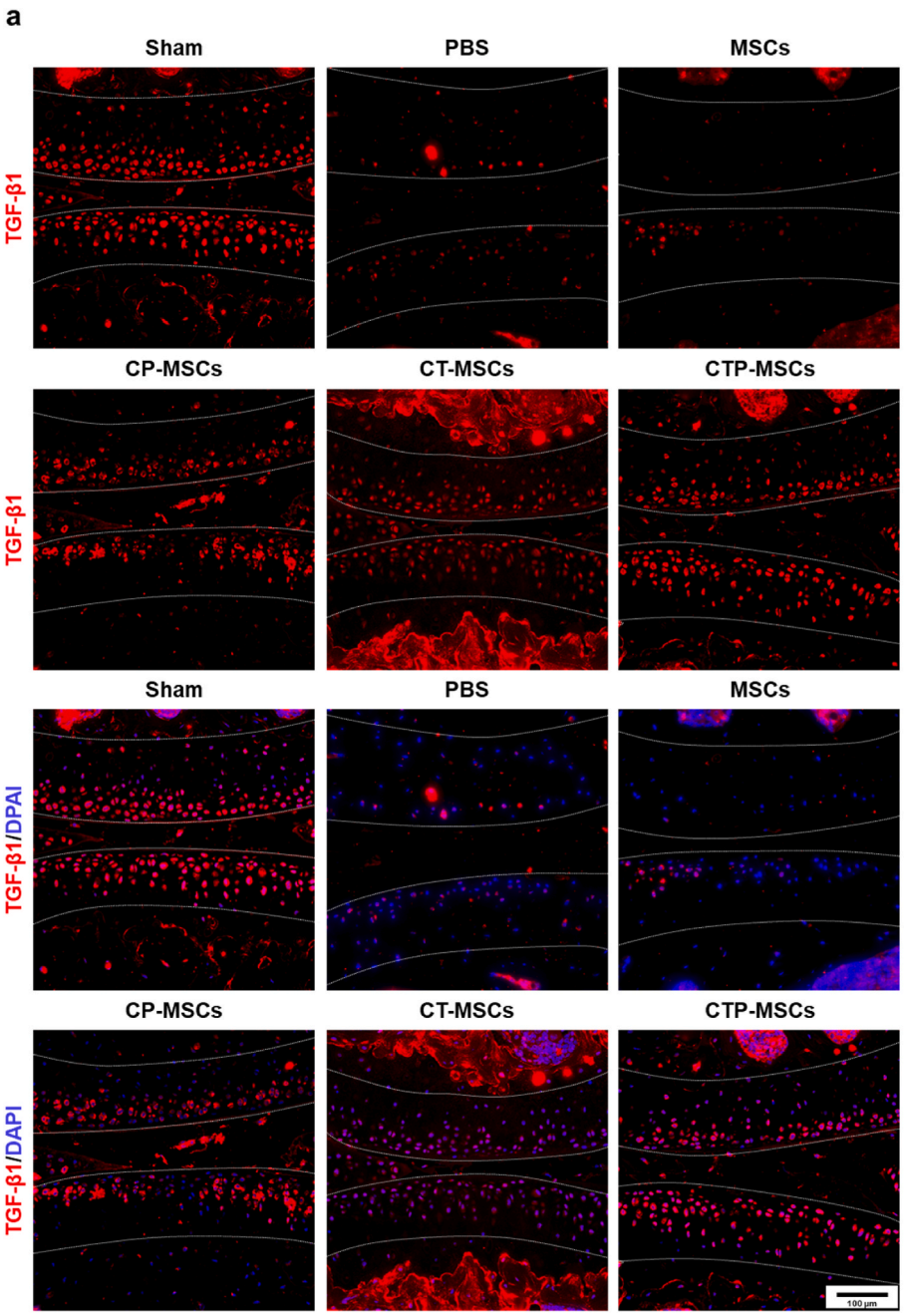

Fig. 8. Immunofluorescence staining of TGF-β1 in knee joints at 10 weeks post-surgery. The expression of TGF-β1 were higher in NP-engineered MSCs groups relative to pure MSCs and control groups. Specifically, the expression levels of TGF-β1 were similar between CTP-MSCs and sham groups. The cartilage areas were highlighted by white dotted lines.

the expression level of MMP-13, suggesting that the matrix degradation of OA cartilage was relived after treatments (Fig. 9). Overall, CTP-MSCs were the best against cartilage erosion among all NP-engineered MSCs.

In addition, we investigated the distribution of CTP-MSCs and pure MSCs after intraarticular injection in vivo. We found that the red fluorescence intensity (DiD-labeled MSCs) at the cartilage injured site in CTP-MSC group was stronger than that of pure MSC group (Fig. S6). This result indicated that more CTP-MSCs were presented at cartilage injured site due to their stronger cell migration ability relative to pure MSCs. Further, histological analysis showed that the main organs of mice after treatments were normal in all groups (Fig. S7). Moreover, the results of blood biochemical tests had no significant differences among all groups (Fig. S8), indicating that the NP-engineered MSCs did not influence the liver and kidney function of mice. Hence, CTP-MSCs presented a highly efficiency and safety on the treatment of OA.

4. Discussion

Despite the advantages of MSCs in relieving symptoms and improving functions of joints, concerns about whether MSCs could repair damaged cartilage are growing in OA therapy. Recent three randomized controlled trials [18–20] revealed that no changes were observed in the whole-organ MRI score (WORMS) of knee cartilage after MSCs treatment, namely, the effect of MSCs on cartilage repair is uncertain. Therefore, enhancing the chondrogenic inductivity of MSCs without affecting their basic functions may be a promising strategy to overcome these drawbacks.

In our approach, we conjugated CuS NPs with TGF-β1 pDNA to

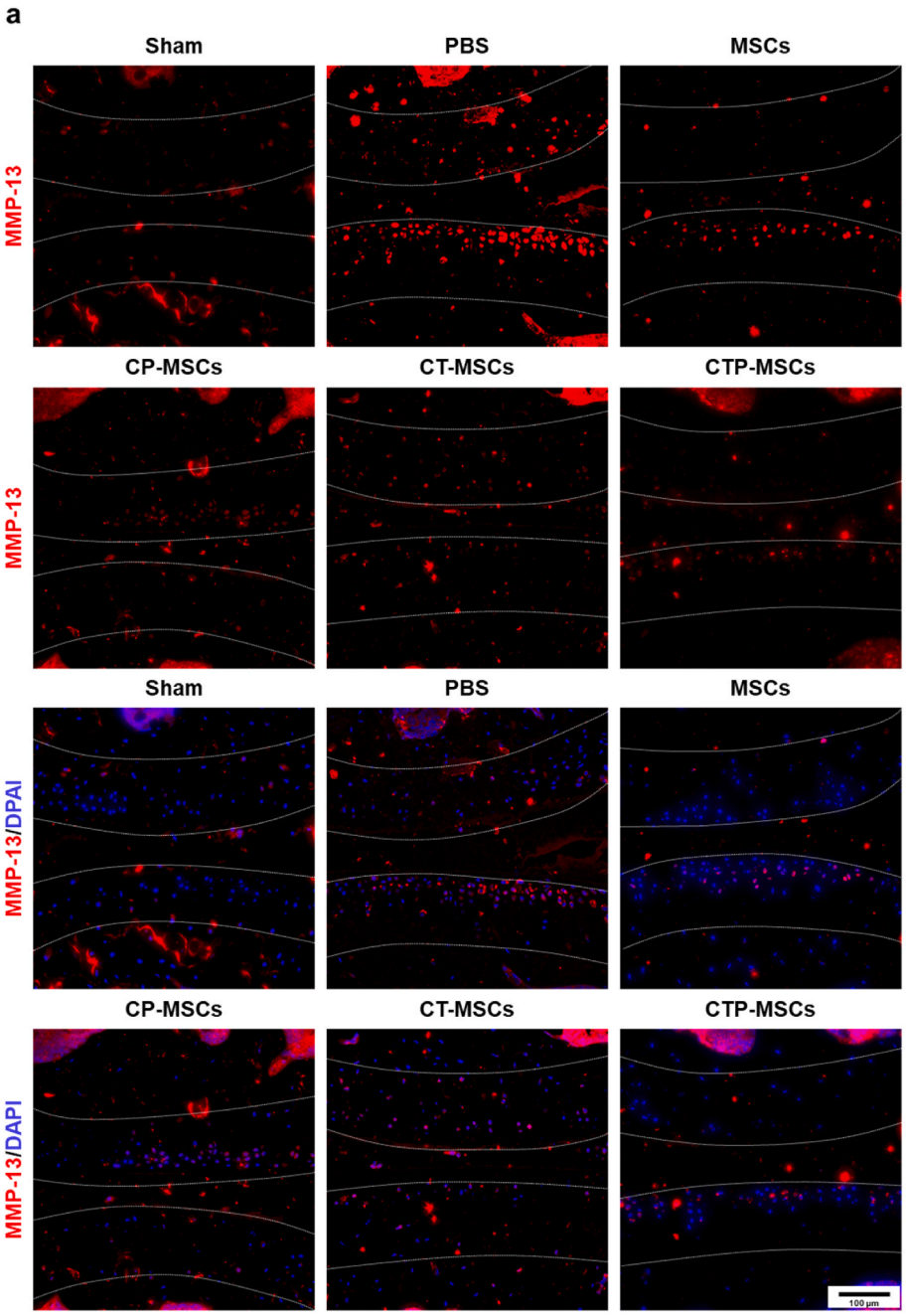

Fig. 9. Immunofluorescence staining of MMP-13 in knee joints at 10 weeks post-surgery. The expression of MMP-13 was lower in NP-engineered MSCs groups relative to MSCs and PBS groups. The cartilage areas were highlighted by white dotted lines.

enhance the chondrogenesis of the NP-engineered MSCs. Moreover, the NPs were modified with PC on the surface, allowing the NPs to enhance MSCs with low cytotoxicity. We demonstrated that the new CTP-MSCs indeed migrated to cartilage lesions and enhanced cartilage repair in OA mice after intraarticular injection.

Cu is an essential trace element in the human body with multiple biofunctions [25,38–40]. However, excessive Cu ions are toxic to mammal cells due to that oxidative pathway can be activated by high concentration of Cu ions [41,42]. Hence, the direct application of Cu ions in tissue engineering is restricted [43]. Compared to Cu ions, Cu-based NPs (e.g., CuS and CuO NPs) are more structurally and chemically stable. They gradually release Cu ions in a mild manner [44]. We showed that both CuS and CuS@PC NPs within proper concentrations were safe and could promote the proliferation of MSCs (Fig. 2). Our results were consistent with previous reports that Cu could promote chondrocytes proliferation by enhancing the synthesis of insulin-like growth factor 1 (IGF-1) [45]. MSCs are expected to migrate to cartilage lesions after injection. Previous studies demonstrated that Cu ions within controlled dosage could promote the migration of MSCs [46,47]. CuS NP anchored to graphene oxide nanosheets also accelerate cell migration of fibroblasts and endothelial cells. CuS NP also accelerate wound healing in methicillin-resistant *Staphylococcus aureus* (MRSA)-infected wounds [36]. Similarly, our NP-engineered C-MSCs and CP-MSCs exhibited a stronger migratory ability relative to pure MSCs in vitro (Fig. 3). More importantly, more CTP-MSCs were observed at cartilage damaged site compared to pure MSCs after 48 h of injection in vivo (Fig. S6).

Cu is also important in cartilage homeostasis. Cu acts a cofactor for

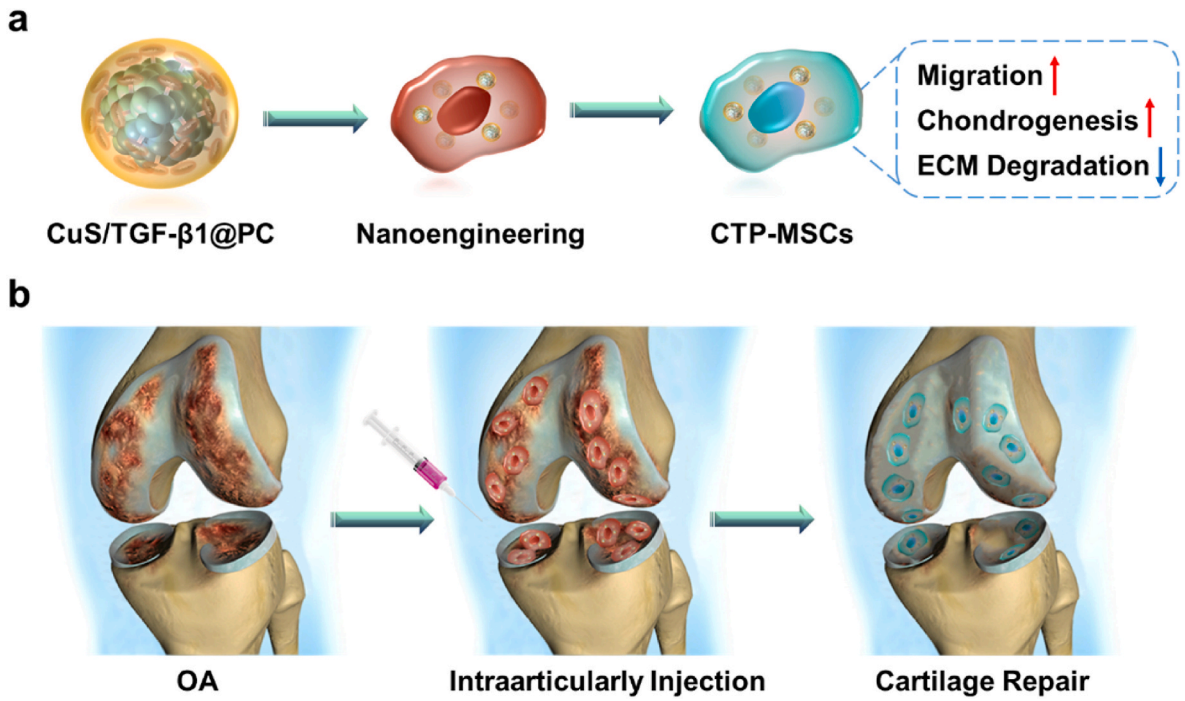

Fig. 10. Schematic illustration of the applications of biomimetic CuS NP-engineered MSCs for OA treatment. (a) CuS NPs loaded with pDNA encoding TGF-β1 were modified with PC (favoring nanoengineering of MSCs). The resultant CuS/TGF-β1@PC (termed CTP) NPs were used to engineer MSCs. The resultant CTP-MSCs exhibited enhanced bioactive properties, including cell migration, chondrogenesis, and inhibition of ECM degradation. (b) In an early OA model, CTP-MSCs were intraarticularly injected into the knee and significantly promoted articular cartilage regeneration, leading to a successful OA therapy.

the cross-linking effect of elastic fibers and collagen [48]. It activates lysyl oxidase, a cuproenzyme, to maintain the functional integrity of articular cartilage through participating in the formation of GAG and collagen [48]. Previously, we found that Cu ions and CuO NPs could promote chondrogenesis of MSCs by up-regulating chondrogenic genes expression and matrix synthesis [25,49]. Other researchers reported that Cu enhanced the secretion of TGF-β [50] to facilitate MSC chondrogenesis and to promote and maintain chondrogenic phenotype of chondrocytes [45,51,52]. In this study, the expression levels of chondrogenic genes, including SOX-6, SOX-9, aggrecan and Col-2a1, were significantly up-regulated in CTP-MSCs group compared to pure MSCs group, indicating the synergistic chondrogenic inductivity of Cu and TGF-β1 (Fig. 4). In addition, the NP-engineered MSCs inhibited the matrix degradation of OA chondrocytes (Fig. 5). However, we found that the expression of fibrotic genes (Col-1a1 and Col-1a2) and hypertrophic genes (Col-10a1 and MMP-13) were higher in CP-MSCs relative to pure MSCs. Fibrosis and hypertrophy are involved in the pathological changes of OA cartilage degeneration [53,54]. Interestingly, the fibrotic and hypertrophic genes expression had no difference between CTP-MSCs and pure MSCs (Fig. S5).

In recent years, TGF-β1 has used in OA therapy [55,56]. TGF-β1 can inhibit hypertrophy of chondrocytes by inhibiting the activity of MMP family molecular [57] and promoting the generation of GAG and other ECM components [58–60]. Moreover, chondrogenic markers of MSCs can be up-regulated by TGF-β1 [61], which is also confirmed in our study. Although TGF-β1 may induce the expression of Col-1a1 and Col-10a1 [61,62], fibrosis and hypertrophy only occur in cartilage when TGF-β1 is repeatedly injected with a high dosage [62]. These adverse effects of TGF-β1 were not observed in our CTP-MSCs because the transfection efficacy of CTP NPs was high and the NP concentration used in nanoengineering was low. Overall, CTP-MSCs are in favor of OA therapy because they can migrate to cartilage lesions and then differentiate into chondrocytes without causing fibrosis and hypertrophy, resulting in a successful cartilage repair of OA mice (Fig. 6).

5. Conclusion

In summary, we developed nanoengineered MSCs as a new modality for OA treatment. The NP-engineered MSCs bore three highly desired functions for stem cell-based therapy in OA, including accelerated cell migration, enhanced chondrogenesis, and inhibition of extracellular matrix degradation (Fig. 10a). These cartilage-repair-favored features enabled these NP-engineered MSCs to promote cartilage regeneration in OA models with only four intraarticular injections (Fig. 10b). Specifically, CTP-MSCs exhibited the best cartilage repairing effect among all NP-engineered MSCs and did not cause any adverse effects on main organs as well as liver and kidney functions. Hence, the nanoengineered MSCs could provide an efficient and safe strategy to overcome limitations of current stem cell therapy and achieve a successful OA treatment.

CRediT authorship contribution statement

Yu Cai: Writing – original draft, Methodology, Investigation, Visualization. **Cuixi Wu:** Methodology, Investigation. **Qianhua Ou:** Methodology, Investigation. **Muhui Zeng:** Methodology, Investigation. **Song Xue:** Methodology, Investigation. **Jieli Chen:** Methodology, Investigation. **Yao Lu:** Conceptualization, Funding acquisition, Supervision, Writing – review & editing. **Changhai Ding:** Conceptualization, Funding acquisition, Supervision, Writing – review & editing.

Declaration of competing interest

The authors declare no conflict of interest.

Acknowledgements

This study was supported by National Natural Science Foundation of China (81902198, 81974342, 82172391), Guangdong Basic and Applied Basic Research Foundation (2020A1515010398), China National Postdoctoral Program for Innovative Talents (BX20190150),

China Postdoctoral Science Foundation (2019M662980), and President Foundation of Zhujiang Hospital, Southern Medical University (yzjj2018rc09).

Appendix A. Supplementary data

Supplementary data to this article can be found online at https://doi.org/10.1016/j.bioactmat.2022.04.021.

References

[1] S. Glyn-Jones, A.J.R. Palmer, R. Agricola, A.J. Price, T.L. Vincent, H. Weinans, A. J. Carr, Osteoarthritis, Lancet 386 (9991) (2015) 376–387.
[2] R. Barnett, Osteoarthritis, Lancet 391 (10134) (2018) 1985.
[3] A. Guermazi, T. Neogi, J.N. Katz, C.K. Kwoh, P.G. Conaghan, D.T. Felson, F. W. Roemer, Intra-articular corticosteroid injections for the treatment of hip and knee osteoarthritis-related pain: considerations and controversies with a focus on imaging- scientific expert panel, Radiology 297 (3) (2020) 503–512.
[4] P. Cao, Y. Li, Y. Tang, C. Ding, D.J. Hunter, Pharmacotherapy for knee osteoarthritis: current and emerging therapies, Expet Opin. Pharmacother. 21 (7) (2020) 797–809.
[5] X. Cai, S. Yuan, Y. Zeng, C. Wang, N. Yu, C. Ding, New trends in pharmacological treatments for osteoarthritis, Front. Pharmacol. 12 (2021) 645842.
[6] D.K. Bae, K.H. Yoon, S.J. Song, Cartilage healing after microfracture in osteoarthritic knees, Arthroscopy 22 (4) (2006) 367–374.
[7] P.C. Kreuz, M.R. Steinwachs, C. Erggelet, S.J. Krause, G. Konrad, M. Uhl, N. Südkamp, Results after microfracture of full-thickness chondral defects in different compartments in the knee, Osteoarthritis Cartilage 14 (11) (2006) 1119–1125.
[8] D.B.F. Saris, J. Vanlauwe, J. Victor, M. Haspl, M. Bohnsack, Y. Fortems, B. Vandekerckhove, K.F. Almqvist, T. Claes, F. Handelberg, K. Lagae, J. van der Bauwhede, H. Vandenneucker, K.G.A. Yang, M. Jelic, R. Verdonk, N. Veulemans, J. Bellemans, F.P. Luyten, Characterized chondrocyte implantation results in better structural repair when treating symptomatic cartilage defects of the knee in a randomized controlled trial versus microfracture, Am. J. Sports Med. 36 (2) (2008) 235–246.
[9] G. Bentley, L.C. Biant, S. Vijayan, S. Macmull, J.A. Skinner, R.W.J. Carrington, Minimum ten-year results of a prospective randomised study of autologous chondrocyte implantation versus mosaicplasty for symptomatic articular cartilage lesions of the knee, J. Bone Joint Surg. Br. 94 (4) (2012) 504–509.
[10] L. Peterson, T. Minas, M. Brittberg, A. Nilsson, E. Sjögren-Jansson, A. Lindahl, Two- to 9-year outcome after autologous chondrocyte transplantation of the knee, Clin. Orthop. Relat. Res. 374 (2000) 212–234.
[11] E.A. Makris, A.H. Gomoll, K.N. Malizos, J.C. Hu, K.A. Athanasiou, Repair and tissue engineering techniques for articular cartilage, Nat. Rev. Rheumatol. 11 (1) (2015) 21–34.
[12] M.F. Pittenger, A.M. Mackay, S.C. Beck, R.K. Jaiswal, R. Douglas, J.D. Mosca, M. A. Moorman, D.W. Simonetti, S. Craig, D.R. Marshak, Multilineage potential of adult human mesenchymal stem cells, Science 284 (5411) (1999) 143–147.
[13] M. Ullah, D.D. Liu, A.S. Thakor, Mesenchymal stromal cell homing: mechanisms and strategies for improvement, iScience 15 (2019) 421–438.
[14] J.M. Karp, G.S. Leng Teo, Mesenchymal stem cell homing: the devil is in the details, Cell Stem Cell 4 (3) (2009) 206–216.
[15] R. Zhang, J. Ma, J. Han, W. Zhang, J. Ma, Mesenchymal stem cell related therapies for cartilage lesions and osteoarthritis, Am. J. Transl. Res. 11 (10) (2019) 6275–6289.
[16] D.S. Jevotovsky, A.R. Alfonso, T.A. Einhorn, E.S. Chiu, Osteoarthritis and stem cell therapy in humans: a systematic review, Osteoarthritis Cartilage 26 (6) (2018) 711–729.
[17] J. Wang, L. Zhou, Y. Zhang, L. Huang, Q. Shi, Mesenchymal stem cells - a promising strategy for treating knee osteoarthritis, Bone Joint Res. 9 (10) (2020) 719–728.
[18] P.K. Gupta, A. Chullikana, M. Rengasamy, N. Shetty, V. Pandey, V. Agarwal, S. Y. Wagh, P.K. Vellotare, D. Damodaran, P. Viswanathan, C. Thej, S. Balasubramanian, A.S. Majumdar, Efficacy and safety of adult human bone marrow-derived, cultured, pooled, allogeneic mesenchymal stromal cells (Stempeucel®): preclinical and clinical trial in osteoarthritis of the knee joint, Arthritis Res. Ther. 18 (1) (2016) 301.
[19] J.M. Lamo-Espinosa, G. Mora, J.F. Blanco, F. Granero-Moltó, J.M. Nuñez-Córdoba, C. Sánchez-Echenique, J.M. Bondía, J.D. Aquerreta, E.J. Andreu, E. Ornilla, E. M. Villarón, A. Valentí-Azcárate, F. Sánchez-Guijo, M.C. Del Cañizo, J.R. Valentí-Nin, F. Prósper, Intra-articular injection of two different doses of autologous bone marrow mesenchymal stem cells versus hyaluronic acid in the treatment of knee osteoarthritis: multicenter randomized controlled clinical trial (phase I/II), J. Transl. Med. 14 (1) (2016) 246.
[20] J. Matas, M. Orrego, D. Amenabar, C. Infante, R. Tapia-Limonchi, M.I. Cadiz, F. Alcayaga-Miranda, P.L. González, E. Muse, M. Khoury, F.E. Figueroa, F. Espinoza, Umbilical cord-derived mesenchymal stromal cells (MSCs) for knee osteoarthritis: repeated MSC dosing is superior to a single MSC dose and to hyaluronic acid in a controlled randomized phase I/II trial, Stem Cells Transl. Med. 8 (3) (2019) 215–224.
[21] C.-W. Ha, Y.-B. Park, S.H. Kim, H.-J. Lee, Intra-articular mesenchymal stem cells in osteoarthritis of the knee: a systematic review of clinical outcomes and evidence of cartilage repair, Arthroscopy 35 (1) (2019).
[22] F. Barry, M. Murphy, Mesenchymal stem cells in joint disease and repair, Nat. Rev. Rheumatol. 9 (10) (2013) 584–594.
[23] R. Gerter, J. Kruegel, N. Miosge, New insights into cartilage repair - the role of migratory progenitor cells in osteoarthritis, Matrix Biol. 31 (3) (2012) 206–213.
[24] T. Vinardell, E.J. Sheehy, C.T. Buckley, D.J. Kelly, A comparison of the functionality and in vivo phenotypic stability of cartilaginous tissues engineered from different stem cell sources, Tissue Eng. A 18 (11–12) (2012) 1161–1170.
[25] C. Xu, J. Chen, L. Li, X. Pu, X. Chu, X. Wang, M. Li, Y. Lu, X. Zheng, Promotion of chondrogenic differentiation of mesenchymal stem cells by copper: implications for new cartilage repair biomaterials, Mater. Sci. Eng. C Mater. Biol. Appl. 93 (2018) 106–114.
[26] J.N. van der Veen, J.P. Kennelly, S. Wan, J.E. Vance, D.E. Vance, R.L. Jacobs, The critical role of phosphatidylcholine and phosphatidylethanolamine metabolism in health and disease, Biochim. Biophys. Acta Biomembr. 1859 (9 Pt B) (2017) 1558–1572.
[27] W. Wang, X. Cheng, J. Liao, Z. Lin, L. Chen, D. Liu, T. Zhang, L. Li, Y. Lu, H. Xia, Synergistic photothermal and photodynamic therapy for effective implant-related bacterial infection elimination and biofilm disruption using CuS nanoparticles, ACS Biomater. Sci. Eng. 5 (11) (2019) 6243–6253.
[28] Y. Lu, L. Li, Z. Lin, L. Wang, L. Lin, M. Li, Y. Zhang, Q. Yin, Q. Li, H. Xia, A new treatment modality for rheumatoid arthritis: combined photothermal and photodynamic therapy using Cu S nanoparticles, Adv. Healthc. Mater. 7 (14) (2018), e1800013.
[29] T.-y. Cheang, B. Tang, A.-w. Xu, G.-q. Chang, Z.-j. Hu, W.-l. He, Z.-h. Xing, J.-b. Xu, M. Wang, S.-m. Wang, Promising plasmid DNA vector based on APTES-modified silica nanoparticles, Int. J. Nanomed. 7 (2012) 1061–1067.
[30] M. Dominici, K. Le Blanc, I. Mueller, I. Slaper-Cortenbach, F. Marini, D. Krause, R. Deans, A. Keating, D. Prockop, E. Horwitz, Minimal criteria for defining multipotent mesenchymal stromal cells, Int. Soc. Cell. Ther. Position Statement, Cytother. 8 (4) (2006) 315–317.
[31] Y. Lu, L. Li, Y. Zhu, X. Wang, M. Li, Z. Lin, X. Hu, Y. Zhang, Q. Yin, H. Xia, C. Mao, Multifunctional copper-containing carboxymethyl chitosan/alginate scaffolds for eradicating clinical bacterial infection and promoting bone formation, ACS Appl. Mater. Interfaces 10 (1) (2018) 127–138.
[32] Y. Cao, S.a. Tang, X. Nie, Z. Zhou, G. Ruan, W. Han, Z. Zhu, C. Ding, Decreased miR-214-3p activates NF-κB pathway and aggravates osteoarthritis progression, EBioMedicine 65 (2021) 103283.
[33] S.S. Glasson, M.G. Chambers, W.B. Van Den Berg, C.B. Little, The OARSI histopathology initiative - recommendations for histological assessments of osteoarthritis in the mouse, Osteoarthritis Cartilage 18 (Suppl 3) (2010) S17–S23.
[34] N. Yanasarn, B. Sloat, Z. Cui, Nanoparticles engineered from lecithin-in-water emulsions as a potential delivery system for docetaxel, 1 379, 2009, pp. 174–180.
[35] K. Hu, S. Cao, F. Hu, J. Feng, Enhanced oral bioavailability of docetaxel by lecithin nanoparticles: preparation, in vitro, and in vivo evaluation 7, 2012, pp. 3537–3545.
[36] W. Wang, B. Li, H. Yang, Z. Lin, L. Chen, Z. Li, J. Ge, T. Zhang, H. Xia, L. Li, Y. Lu, Efficient elimination of multidrug-resistant bacteria using copper sulfide nanozymes anchored to graphene oxide nanosheets, Nano Res. 13 (8) (2020) 2156–2164.
[37] D.H. Vynios, Metabolism of cartilage proteoglycans in health and disease, BioMed Res. Int. 2014 (2014) 452315.
[38] E. Tomaszewska, P. Dobrowolski, M. Kwiecień, A. Winiarska-Mieczan, A. Tomczyk, Siemowit Muszyński, The influence of the dietary Cu-Glycine complex on the histomorphology of cancellous bone, articular cartilage, and growth plate as well as bone mechanical and geometric parameters is Dose Dependent, 1 178, 2017, pp. 54–63.
[39] S. Li, H. Xie, S. Li, Y.J. Kang, Copper stimulates growth of human umbilical vein endothelial cells in a vascular endothelial growth factor-independent pathway, Exp. Biol. Med. (Maywood) 237 (1) (2012) 77–82.
[40] A. Ali, M. Ershad, V.K. Vyas, S.K. Hira, P.P. Manna, B.N. Singh, S. Yadav, P. Srivastava, S.P. Singh, R. Pyare, Studies on effect of CuO addition on mechanical properties and in vitro cytocompatibility in 1393 bioactive glass scaffold, Mater. Sci. Eng. C Mater. Biol. Appl. 93 (2018) 341–355.
[41] H. Zhang, Z. Ji, T. Xia, H. Meng, C. Low-Kam, R. Liu, S. Pokhrel, S. Lin, X. Wang, Y.-P. Liao, M. Wang, L. Li, R. Rallo, R. Damoiseaux, D. Telesca, L. Mädler, Y. Cohen, J. I. Zink, A.E. Nel, Use of metal oxide nanoparticle band gap to develop a predictive paradigm for oxidative stress and acute pulmonary inflammation, ACS Nano 6 (5) (2012) 4349–4368.
[42] A.M. Studer, L.K. Limbach, L. Van Duc, F. Krumeich, E.K. Athanassiou, L.C. Gerber, H. Moch, W.J. Stark, Nanoparticle cytotoxicity depends on intracellular solubility: comparison of stabilized copper metal and degradable copper oxide nanoparticles, Toxicol. Lett. 197 (3) (2010) 169–174.
[43] I. Scheiber, R. Dringen, J.F.B. Mercer, Copper: effects of deficiency and overload, Met. Ions Life Sci. 13 (2013) 359–387.
[44] K. Midander, P. Cronholm, H.L. Karlsson, K. Elihn, L. Möller, C. Leygraf, I. O. Wallinder, Surface characteristics, copper release, and toxicity of nano- and micrometer-sized copper and copper(II) oxide particles: a cross-disciplinary study, Small 5 (3) (2009) 389–399.
[45] J. Wang, X. Zhu, X. Li, W. Wang, X. Wang, L. Liu, Q. Deng, G. Bai, J. Wang, H. Feng, Z. Wang, G. Liu, Effects of copper on proliferation and autocrine secretion of insulin-like growth factor-1 (IGF-1) and IGF-binding protein-3 (IGFBP-3) in chondrocytes from newborn pigs in vitro, Biol. Trace Elem. Res. 144 (1–3) (2011) 588–596.
[46] X. Chen, J.-G. Hu, Y.-Z. Huang, S. Li, S.-F. Li, M. Wang, H.-W. Xia, J. Li-Ling, H.-Q. Xie, Copper promotes the migration of bone marrow mesenchymal stem cells via

Rnd3-dependent cytoskeleton remodeling, J. Cell. Physiol. 235 (1) (2020) 221–231.
[47] M. Milewska, A. Burdzińska, K. Zielniok, K. Siennicka, S. Struzik, P. Zielenkiewicz, L. Pączek, Copper does not induce tenogenic differentiation but promotes migration and increases lysyl oxidase activity in adipose-derived mesenchymal stromal cells, Stem Cell. Int. 2020 (2020) 9123281.
[48] E.A. Makris, R.F. MacBarb, D.J. Responte, J.C. Hu, K.A. Athanasiou, A copper sulfate and hydroxylysine treatment regimen for enhancing collagen cross-linking and biomechanical properties in engineered neocartilage, Faseb. J. 27 (6) (2013) 2421–2430.
[49] Y. Lu, J. Chen, L. Li, Y. Cao, Y. Zhao, X. Nie, C. Ding, Hierarchical functional nanoparticles boost osteoarthritis therapy by utilizing joint-resident mesenchymal stem cells, J. Nanobiotechnol. 20 (1) (2022) 89.
[50] X. Zhu, J. Wang, G. Xie, H. Feng, X. Li, L. Liu, X. Wang, D. Li, Z. Liu, J. Qian, Z. Wang, G. Liu, Effect of copper on the expression of TGF-β in incubated chondrocytes of newborn pigs, Biol. Trace Elem. Res. 143 (3) (2011) 1461–1469.
[51] I. Madzovska-Malagurski, M. Vukasinovic-Sekulic, D. Kostic, S. Levic, Towards antimicrobial yet bioactive Cu-alginate hydrogels, Biomed. Mater. 11 (3) (2016), 035015.
[52] Y. Wang, W. Zhang, Q. Yao, Copper-based biomaterials for bone and cartilage tissue engineering, J. Orthop. Translat. 29 (2021) 60–71.
[53] X. Wang, P.A. Manner, A. Horner, L. Shum, R.S. Tuan, G.H. Nuckolls, Regulation of MMP-13 expression by RUNX2 and FGF2 in osteoarthritic cartilage, Osteoarthritis Cartilage 12 (12) (2004) 963–973.
[54] S. Kamekura, K. Hoshi, T. Shimoaka, U. Chung, H. Chikuda, T. Yamada, M. Uchida, N. Ogata, A. Seichi, K. Nakamura, H. Kawaguchi, Osteoarthritis development in novel experimental mouse models induced by knee joint instability, Osteoarthritis Cartilage 13 (7) (2005) 632–641.
[55] B. Lee, J. Parvizi, D. Bramlet, D.W. Romness, A. Guermazi, M. Noh, N. Sodhi, A. Khlopas, M.A. Mont, Results of a phase II study to determine the efficacy and safety of genetically engineered allogeneic human chondrocytes expressing TGF-β1, J. Knee Surg. 33 (2) (2020) 167–172.
[56] M.-K. Kim, C.-W. Ha, Y. In, S.-D. Cho, E.-S. Choi, J.-K. Ha, J.-H. Lee, J.-D. Yoo, S.-I. Bin, C.-H. Choi, H.-S. Kyung, M.-C. Lee, A multicenter, double-blind, phase III clinical trial to evaluate the efficacy and safety of a cell and gene therapy in knee osteoarthritis patients, Hum. Gene. Ther. Clin. Dev. 29 (1) (2018) 48–59.
[57] C. Xu, B. Oyajobi, A. Frazer, L. Kozaci, R. Russell, A.J.E. Hollander, Effects of growth factors and interleukin-1 alpha on proteoglycan and type II collagen turnover in bovine nasal and articular chondrocyte pellet cultures, 8 137, 1996, pp. 3557–3565.
[58] R.T. Ballock, A. Heydemann, L.M. Wakefield, K.C. Flanders, A.B. Roberts, M. B. Sporn, TGF-beta 1 prevents hypertrophy of epiphyseal chondrocytes: regulation of gene expression for cartilage matrix proteins and metalloproteases, Dev. Biol. 158 (2) (1993) 414–429.
[59] S. Park, A. Bello, Y. Arai, J. Ahn, D. Kim, K.-Y. Cha, I. Baek, H. Park, S.-H. Lee, Functional duality of chondrocyte hypertrophy and biomedical application trends in osteoarthritis, Pharmaceutics 13 (8) (2021).
[60] A.P. van Caam, W. Madej, H.M. van Beuningen, E.N. Blaney Davidson, P.M. van der Kraan, TGF-beta blocks chondrocyte hypertrophy and maintains cell viability in cultured cartilage explants but does not protect against proteoglycan loss, Osteoarthritis Cartilage 23 (2015) A137–A138.
[61] N. Kovermann, V. Basoli, E. Della Bella, M. Alini, C. Lischer, H. Schmal, E. Kubosch, M.J.C. Stoddart, BMP2 and TGF-β Cooperate differently during synovial-derived Stem-Cell Chondrogenesis in a Dexamethasone-Dependent Manner, 6 8, 2019.
[62] W. Border, N. Noble, Transforming growth factor beta in tissue fibrosis 331 (19) (1994) 1286–1292.